Technical Report*

Neuronal Rhythmicity and its Rate Variability†

Roberto Martin del Campo Vera[1‡], **Edmond Jonckheere**[2§]

[1] *Ming Hsieh Department of Electrical Engineering, University of Southern California*

[2] *Ming Hsieh Department of Electrical Engineering and the Mathematics Department, University of Southern California, Los Angeles, 90089-2563, California, USA*

Abstract

Rhythmic surface Electromyographic (sEMG) bursts for which their returns occur at irregular times are analyzed and compared among healthy and injured central nervous systems. The rhythmic electrophysiological activity in the present study has been defined as *"Bursting Rate Variability" (BRV)* due to the inherent aperiodicity of successive sEMG bursts, which are concomitant with "doublet" waveforms in the D8 subband of the Daubechies 3 wavelet decomposition of the raw signal. A key element in the analysis is the precise time-localization of D8 doublets that requires a statistical waveform matching between the D8 doublet and the burst in the raw sEMG signal. This study has been conducted over a period of 10 years, in which 7 healthy and 2 unhealthy individuals volunteered and presented a total of ∼8,000 doublets: it was observed that doublets were more prevalent in healthy than unhealthy subjects, and that the probability distribution of return times was best fitted with Normal Mixtures in healthy subjects, compared to the Weibull distribution as the best fit in unhealthy ones based on the corrected Akaike Information Criterion (AICc) for model selection. Finally, the rate in the occurrence of doublets appears to be within 60-88 bursts per minute, suggesting a possible connection between BRV and the heart rate dynamics.

Keywords: Bursting, Central Pattern Generator, Discrete Wavelet Transform, Coherence at a distance, Synchronization, Multi-channel surface electromyography, Return time, Weibull distribution, Normal Mixture distributions

*This technical report is intended to provide further details and augment the abridged manuscript "Bursting Rate Variability"; submitted for review to *IEEE Transactions on Neural Systems & Rehabilitation Engineering, March, 2018*

†This research was supported by the Reorganizational Living Foundation and approved by the Institutional Review Board (IRB) of the University of Southern California. The techniques developed in this paper are covered by *US Provisional Patent Application No. 62/608,474.* Filed Dec 20, 2017.

‡E-mail: mart737@usc.edu

§E-mail: jonckhee@usc.edu. URL: http://eudoxus2.usc.edu

1 Introduction

The surface electromyographic (sEMG) activity recorded along the paraspinal muscles has been seen to present standing wave properties [1, 2] when the research subject is placed in the prone position and is applied light pressure at some specific "gateway" points of the spine (usually the neck and the coccyx) to elicit the oscillation.

The motion usually starts in a chaotic fashion at the distal ends of the spine, propagates caudally, until it settles in a standing wave pattern, which can undergo "period halving bifurcations," transitioning away from chaos [3]. At that stage, no further digital stimulus is required, indicating that the rhythmic movement is innervated by a Central Pattern Generator (CPG) [4, 5], as argued in [1]. A further confirmation of the CPG hypothesis is that two quadriplegic subjects have been able to sustain the so-called *spinal wave* [1, 6, 7].

Besides CPG, another important aspect of this movement is *coherence at a distance*; the antinodes of the wave are indeed in coherent motion, with a wavelength in the order of $\sim$1 m, hence qualifying as *coherence at a distance* [8, 9, 10].

The specificity of this CPG-innervated, coherent motion is confirmed by the Daubechies 3 (db3) wavelet decomposition [11, 12] of the sEMG signal, more specifically, by the *"doublet"* waveforms repeating themselves in an aperiodic fashion in the D8 subband of the wavelet decomposition. Due to surface electromyography being a superposition of multiple Motor Unit Action Potential (MUAP) trains (see [13, Fig. 3-4]), it is still a bit unclear at this stage whether the observed "doublets" are two discharges of motor units firing in unison, or single discharges of coupled motor units firing one after the other (see [14, 15, 16] for further details on the double discharge phenomenon). In either case, the observed doublet waveform conforms to the definition of an *"exceptional doublet"* of [14, Fig. 5B], "exceptional" in the sense of large intradoublet interspike interval. Indeed, the intradoublet interspike interval duration of $\sim$62.5 ms—that we have measured peak-to-peak from the D8 doublet waveform—exceeds the conventional limits of 2-20 ms according to the standardization of doublets set by the American Association of Neuromuscular & Electrodiagnostic Medicine [17]. However, it has been reported in [14] that the standard range of doublets can be exceeded as Piotrkiewicz et al. [14] report exceptional doublets with 37 ms of intradoublet time in the human soleus muscle. Furthermore, the Discrete Wavelet Transform (DWT) has also served to obtain the doublet total time duration [18] of $\sim$125 ms measured from onset to offset of the wavelet waveform at scale 8, which spans the time comprised by two wavelet transform coefficients at this scale.

Besides these early findings, the crucial observation that launched this research is the near-synchrony between the onsets of the doublets observed on the D8 traces and the onsets of the

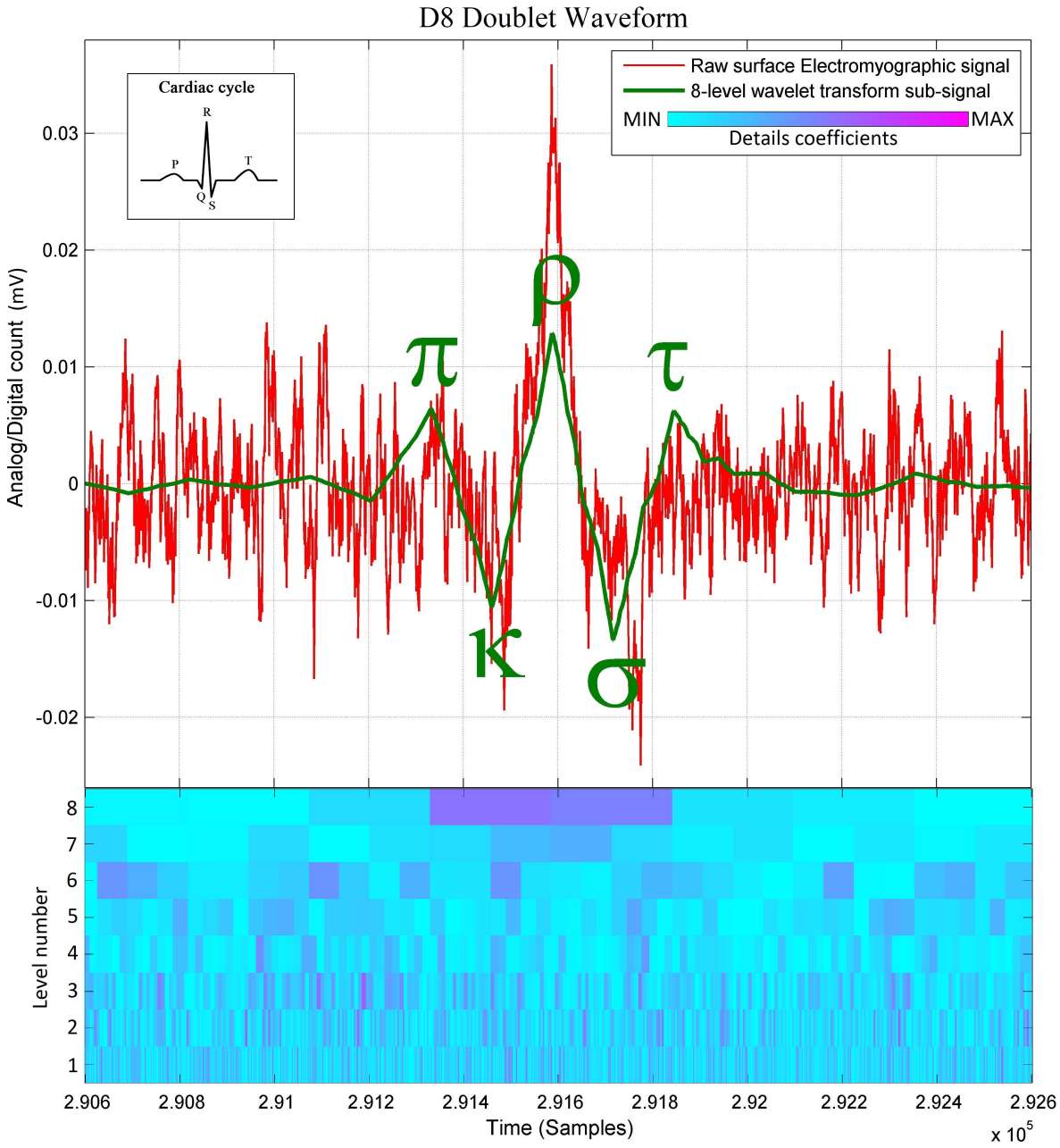

FIGURE 1

Raw paraspinal surface electromyographic signal of a healthy individual, superimposed with its 8-level wavelet transformed sub-signal; its scalogram is shown below: The D8 doublet is a precise sequence of $(+)$ peaks and $(-)$ dips, defined here as the π-κ-ρ-σ-τ sequence because of its similarity with the cardiac cycle. The concordance between the D8 and the burst here appears naturally without preprocessing.

bursts of accrued sEMG activity visible on the raw signal traces, as shown in Figs. 1 and 2. The "nearness" of the time localizations of the doublets and the bursts is crucial here.

By definition of the wavelet decomposition, the repetition of the DWT frame generating the D8 subband is periodic, while the sequence of bursts is not. Therefore, some time-shifting of the

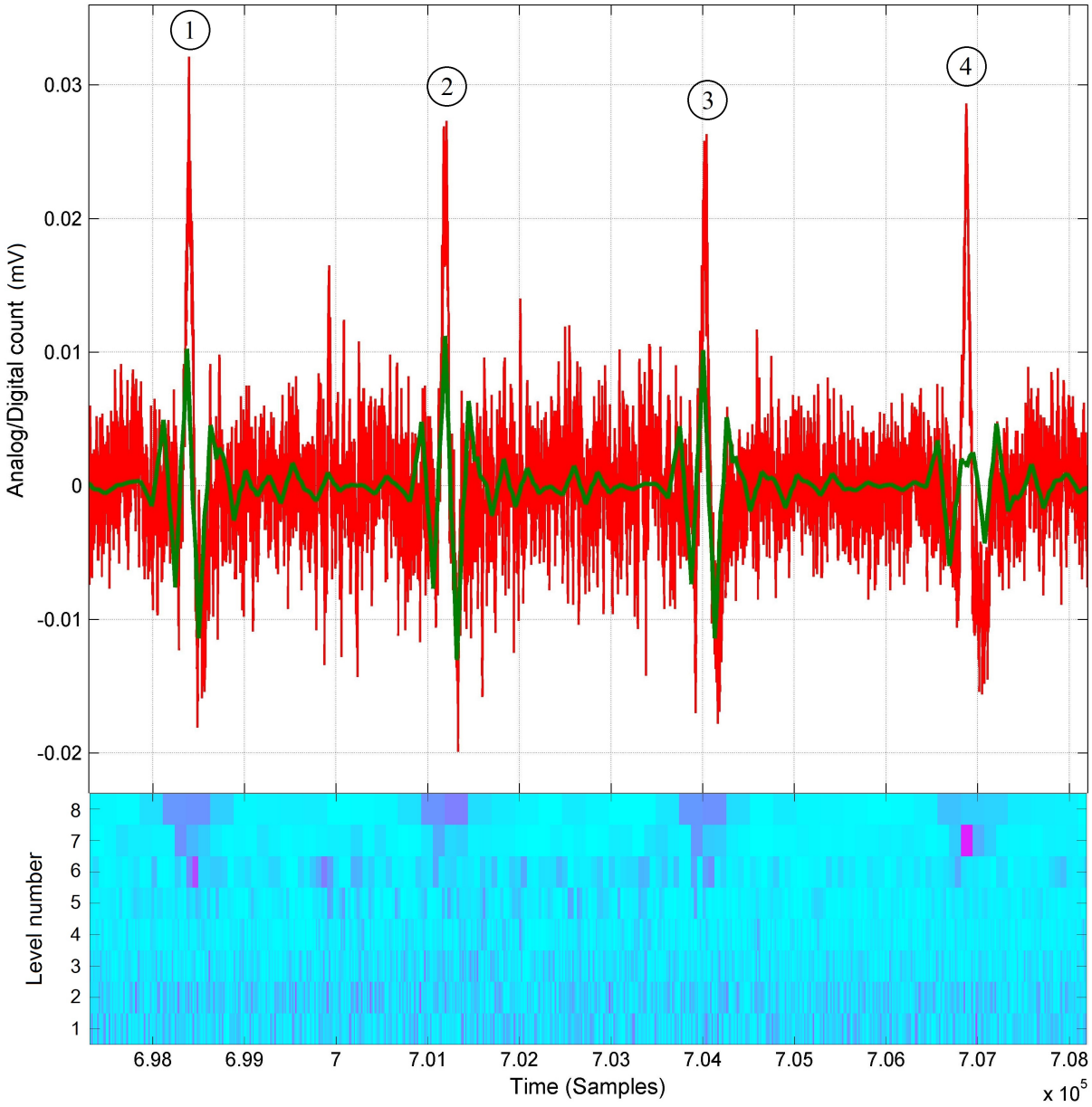

FIGURE 2

Raw thoracic surface electromyographic signal (in red) of control subject #4, superimposed with its 8-level wavelet transformed sub-signal (in green); its scalogram is shown below: Note that at the first, second, and third bursts the matching between the raw sEMG signal and its 8-level sub-signal is better than the one at the fourth burst. The recovery of the matching between the fourth burst and its D8 doublet is shown in Fig. 4, where different time delays are applied before wavelet processing.

raw signal trace is necessary to acquire a good *waveform matching* between a *specific* burst and its D8 doublet. It turns out that this time-shifting is different from one burst to the other, leading to a variability of the time interval between successive bursts, which is referred to as *Bursting Rate Variability (BRV)*.

The empirical distribution of the time intervals between successive bursts differ from one subject to another, but the types of continuous probability distributions already differentiates the BRV of quadriplegic (Figs. 8a and 8b) versus control subjects (Figs. 7a, 7b, 7c, and 7d). The quadriplegic subjects consistently presented the *Weibull* (Type III Extreme Value [19]) distribution as the best fit, and *mixtures of normal* distributions in the case of control subjects, this discrepancy already points to some neurophysiological applications of BRV, but probably more importantly, it could allow for a *dynamical* understanding of the bursting or doublet phenomenon in *abnormal* conditions. The various sEMG signals are indeed generated by some complicated dynamics, nearly impossible to model from "first principles." However, the Generalized Extreme Value (GEV) theory [20] endeavors to identify the *qualitative* properties of such dynamics, no matter how complicated, from the return time of extreme events, like the bursts.

2 Methods

2.1 Methods: control and quadriplegic subjects

For our analysis, a population of 9 volunteers, 7 control (healthy) and 2 quadriplegic subjects (presenting a total of $\sim$8,000 *doublets*) were chosen, the latter subjects with a cervical spinal cord injury at the C5 vertebral level [1, 7].

To draw an objective comparison between the two types of subjects, the subjects with quadriplegia and the healthy ones had their recordings taken during the same session. Before recordings, the subjects had signed the Informed Consent drafted by the investigators and approved by the University Park Campus (UPC) Institutional Review Board (IRB) of the University of Southern California.

2.2 Methods: electrode placement

The data utilized in this investigation have been recorded over a period of a little more than 10 years. All along those recordings, we have followed a consistent recording protocol: Surface electromyography (sEMG) reduced-noise tripolar electrodes ("Uni Patch Tyco EMG Electrodes Round Disk 7500 2.25 diameter Ag snaps") were placed at cervical (C2-C3), thoracic (T4-T6), lumbar (L3), and sacral (S2-S4) positions; all with the same sampling rate of 4,000 samples per second.

The sensitive input prongs of the front-end electronics were initially at a 45-deg. angle with the muscle fibers and subsequently aligned with the back-muscle fibers, without significant difference observed in the results.

2.3 Methods: equipment

The most recent ($<$4 years) recordings were made with an Insight Discover sEMG station together with a Measurement Computing^{TM} USB-1608FS device for analog-to-digital conversion, while the earlier recordings (10 years ago) were done with an Insight Millennium sEMG station interfaced with a Computer Board PCMCIA DAS16/16 card analog-to-digital converter.

2.4 Methods: wavelet transform

We picked up the Daubechies DB3 wavelet decomposition, originally [1] for the motivation that its D8 subband provided the best correlations among the subband signals at different points along the spine (hence promoting the "coherence at a distance" aspect). Later [3], however, it was discovered that under some conditions the D7 subband was preferable.

Parallel to this line of thoughts, it was found by the present and other investigators that the mother function of the DB3 mimics the MUAPs detected by the electrodes [1, 21], which makes the DB3 the ideal tool for picking up relevant waveforms in an otherwise messy sEMG signal corrupted by noise and motion artifacts.

Furthermore, it was found that the D8 of the db3 allowed for accurate localization of doublets most of the times [1, 2, 3]. A wavelet similar to db3, the Daubechies 4 (db4), appears to mimic a doublet but did not provide satisfactory results as it failed to pick up the onset of some bursts as accurately as the db3 did it. Even though the db4 has more rounded crests and troughs, the db3 kernel still adheres more to the shape of observed electromyographic bursts and the exceptional doublets of [14, Fig. 5B] as the amplitude of the first trough in the db3 wavelet is less negative than its second trough as in [14, Fig. 5B]; however, this reverses in the case of the db4 kernel, in which the first trough is more negative than the second one. Another wavelet tested face-to-face against db3, the Daubechies 2 (db2), did not clearly show the bursts start and end points, compared to db3 that allowed better differentiation between two adjacent doublets.

2.5 Methods: waveform matching

To solve the "shift variance" issue of the DWT of many signals [22] causing in our particular application some of the D8 doublets not to have well-defined peaks and dips (see doublet #4 in Fig. 2), or causing the $\pi\kappa\rho\sigma\tau$ peaks and dips to be horizontally offset with respect to the raw sEMG (see the ρ-peak of doublets #1 and #3 in Fig. 2), we shift the sampling times of the

wavelet coefficients by delaying the time at which the DWT begins. This makes the coefficients span different sections of the same raw sEMG signal.

A matching increment of the π-wave, $\pi\kappa$-slope, κ-wave, $\kappa\rho$-slope, ρ-wave, $\rho\sigma$-slope, σ-wave, $\sigma\tau$-slope, and τ-wave with the raw sEMG burst around doublet #4 of Fig. 2 is obtained by omitting the first 20, 40, and 60 samples (see Figs. 3b, 3c, and 3d, respectively) before wavelet processing. This results in recovering the precise peak-dip sequence of the $\pi\kappa\rho\sigma\tau$ complex of doublet #4''' in the raw burst signal, until achieving the benchmark waveform match of Fig. 1.

Due to the periodic nature of the DWT, continuing to delay the signal by omitting the first 80, 100, and 120 samples (see Figs. 3e, 3f, and 3g, respectively) before wavelet processing, results in getting away from and losing the previously recovered peak-dip sequence obtained with doublet #4'''. This implies that the amount of delay is not necessary to be longer than one fourth of the time a single coefficient spans at this particular level, in our case, since an 8-level coefficient spans $\sim$62.5 ms, then a 15 ms delay (omitting th first 60 samples) was enough to recover the $\pi\kappa\rho\sigma\tau$ peak-dip sequence of doublet #4 as shown in Fig. 3d.

As a consequence of the variability in the occurrence of the bursts, the process of delaying the raw sEMG signal before wavelet processing to achieve optimal waveform matching is different from one raw bursting waveform to another one. Fig. 4 shows how the best-suited time delay for doublet #4''' is not the best suited for doublets #1''', #2''', #3''', as compared with doublets #1, #2, #3 of Fig. 2 when no time delay had been applied.

To make the above procedure optimal, the errors of this $\pi\kappa\rho\sigma\tau$ versus raw burst waveform matching are gathered in a multi-objective optimization function, of which the Pareto front is identified using expert rules. If a given delay for the $\pi\kappa\rho\sigma\tau$ waveform parameters is on the Pareto-optimal front as in Fig. 3d, then this provides a good match; whereas if some delays are not on the Pareto-optimal front as those in Figs. 3a, 3b, 3c, 3e, 3f and 3g, then they do not provide a good match.

The expert rules that automatically obtain the minimal error—illustrated in Fig. 3 with vertical lines—between the ρ-wave locations of each D8 doublet and the peak of its raw burst consist of a series of nested conditional statements (*if-then-else* rules) inside a *for* loop, with index value that represents the chronological position of each doublet appearing in the time series, (see flowchart of Fig. 5).

Due to the raw sEMG signal being corrupted with high-frequency noise, and in order to increase the precision in finding the times at local maxima for each D8 doublet, a Savitzky-Golay filter is applied to the raw sEMG before being processed by the expert system. In the present study, three pre-programmed delays of 5 ms, 10 ms, and 15 ms have been entered into

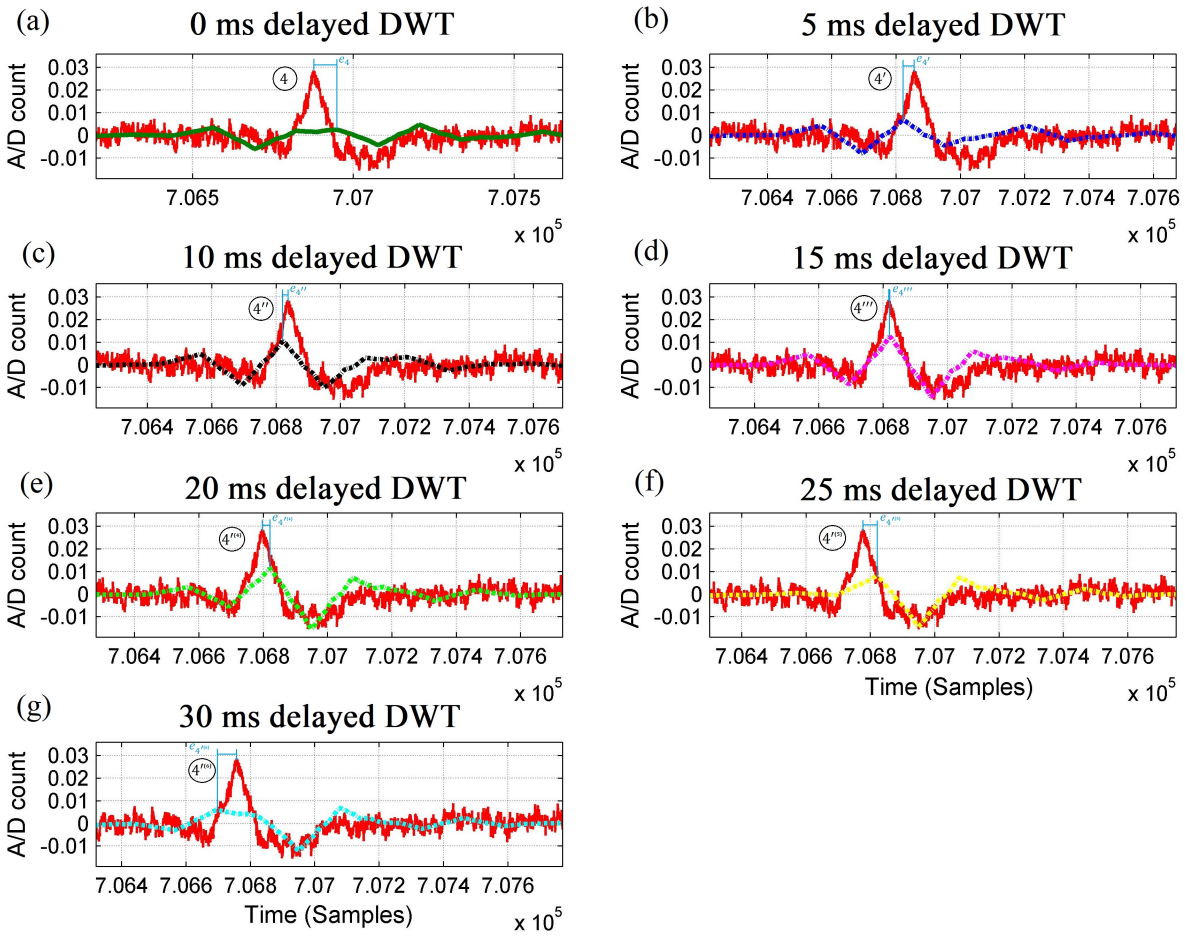

FIGURE 3

Raw thoracic surface electromyographic signal of control subject #4 (in red) centered around doublet #4 of Fig. 2, superimposed with its 8-level wavelet transformed sub-signal when (a) no delay (in dark green), (b) 5 ms delay (in dark blue), (c) 10 ms delay (in black), (d) 15 ms delay (in magenta), (e) 20 ms delay (in light green), (f) 25 ms delay (in yellow), and (g) 30 ms delay (in cyan) is applied to the raw sEMG signal before wavelet processing, where the peak time errors of the ρ-wave are $|e_{4'''}| < |e_{4''}| < |e_{4'^{(4)}}| < |e_{4'}| < |e_{4'^{(5)}}| < |e_{4'^{(6)}}| < |e_4|$: The D8 doublet with the smallest error (#4''') belongs to the Pareto-optimal front, whereas D8 doublets #4, #4', #4'', #4'$^{(4)}$, #4'$^{(5)}$, and #4'$^{(6)}$ do not.

the expert system algorithm as an example to attain the best waveform matching among distinct delays. Fig. 3 shows snapshots of the effect of delaying the sEMG signal every 5 ms delays. Since the DWT is periodic, a complete cycle occurs in 30 ms, thus, guidelines on pre-setting the delay values are in the range from 1 to 30 ms. It is worth noting that the expert system also considers the case of no delay time for the D8 doublets that are naturally matched with the sEMG bursts, which is represented with a zero-delay time.

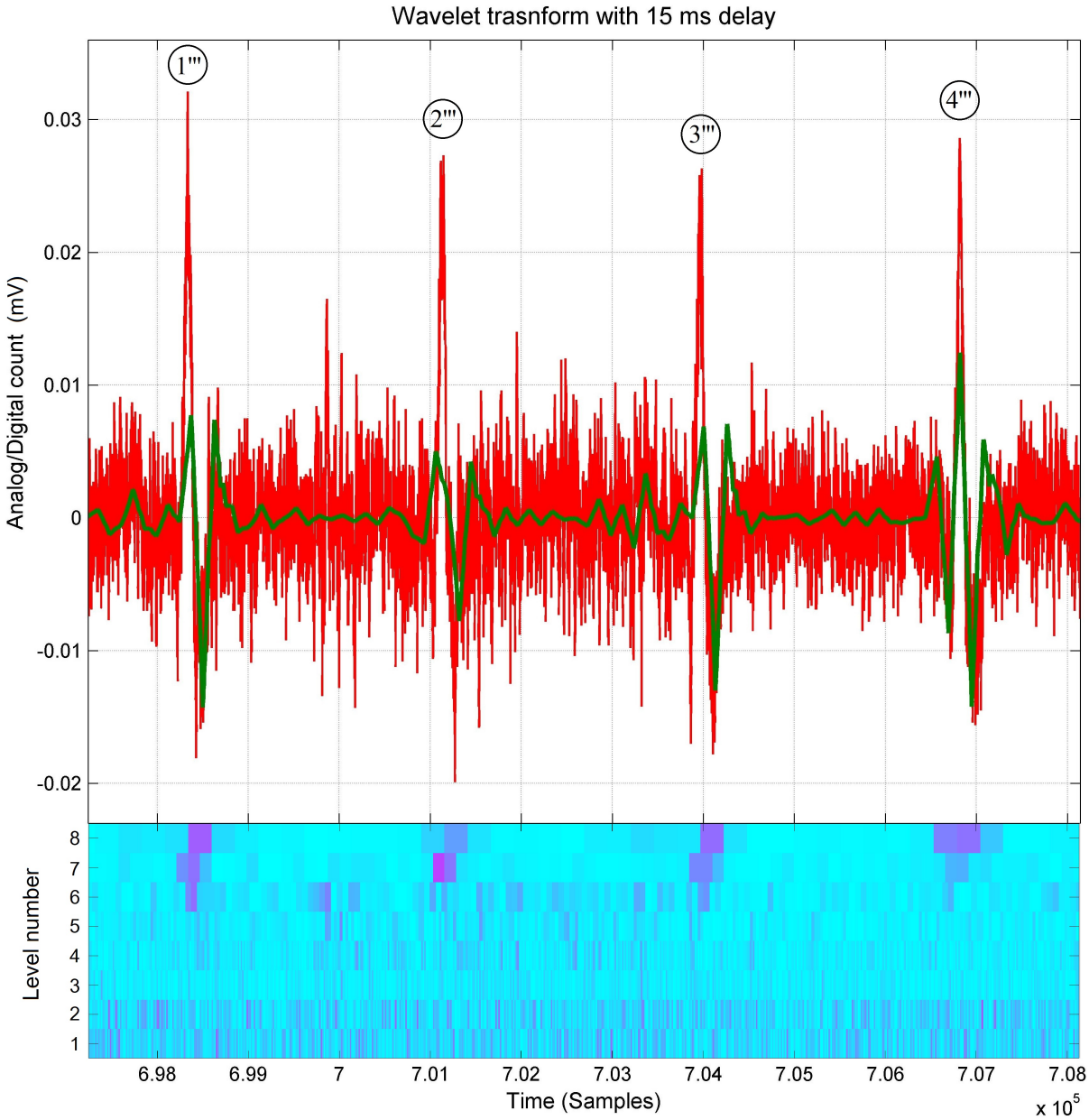

FIGURE 4

Raw thoracic surface electromyographic signal (in red) of subject #4 (control) time-shifted by 15 ms (in red), superimposed with its 8-level wavelet transformed sub-signal (in green); its scalogram is shown below: A time shift of 15 ms (skipping the first 60 samples) on the raw signal before wavelet processing is sufficient for the fourth D8 doublet to better match the raw sEMG signal than when no time shift is applied to the raw signal as in Fig. 2.

The complete sEMG signal processing technique, from data collection to probability distribution fitting, passing through 8-level DWT, delaying, smooth filtering, and including the expert rules is depicted in the flowchart of Fig. 5.

2.6 Methods: empirical vs theoretical distributions and statistical software

There are two ways to construct the histogram of the time between the ρ-waves of successive D8 waveforms, or *"return time"* for short: In one procedure are included in the sample set only those $\rho\rho$-intervals between ρ-waves that are *naturally* matched with their corresponding bursts (without time shifting), discarding those that do not appear to match, such as doublet #4 of Fig. 2. However, some doublets might appear to naturally match with their sEMG bursts—for instance, doublets #1 and #3 of Fig. 2—and considering the ρ-wave locations of these two doublets would add unwanted observational errors to the distribution fit analysis since a better match was found by the expert system (see doublets #1' and #3' of Fig. 6). These undesired errors can be eliminated in the other *"enhanced"* procedure achieved with the expert system and the time-shifted DWT at various time delays; therefore, the latter procedure shall be preferred to increase preciseness in the distribution fitting of return times.

In the *enhanced* procedure, the histogram is constructed with accrued accuracy with $\rho\rho$-intervals after optimal time shifting to match *all* bursts with their respective D8's. The latter, by the same token, also increases the sample size.

The statistical software SAS® Studio 3.4 and JMP Pro 13 (both by the SAS Institute) were used to find the theoretical probability distributions that best fit the frequency histograms of doublet return times based on the (corrected) Akaike Information Criterion (AICc) for model selection; the results are summarized in Table 1. In the case where the Weibull distribution was the best ranked in the AICc sense, it was checked for a goodness of fit using the Cramer-von Mises-W test. As for the best-ranked normal mixture distribution, the Pearson's chi-squared test was used. In both cases, the *null hypothesis* (H_0) states that the observed frequency distribution is consistent with the estimated theoretical distribution, and small p-values ($<$0.05) would reject H_0 in favor of the *alternative hypothesis* (H_1) that the data is not from the theoretical distribution.

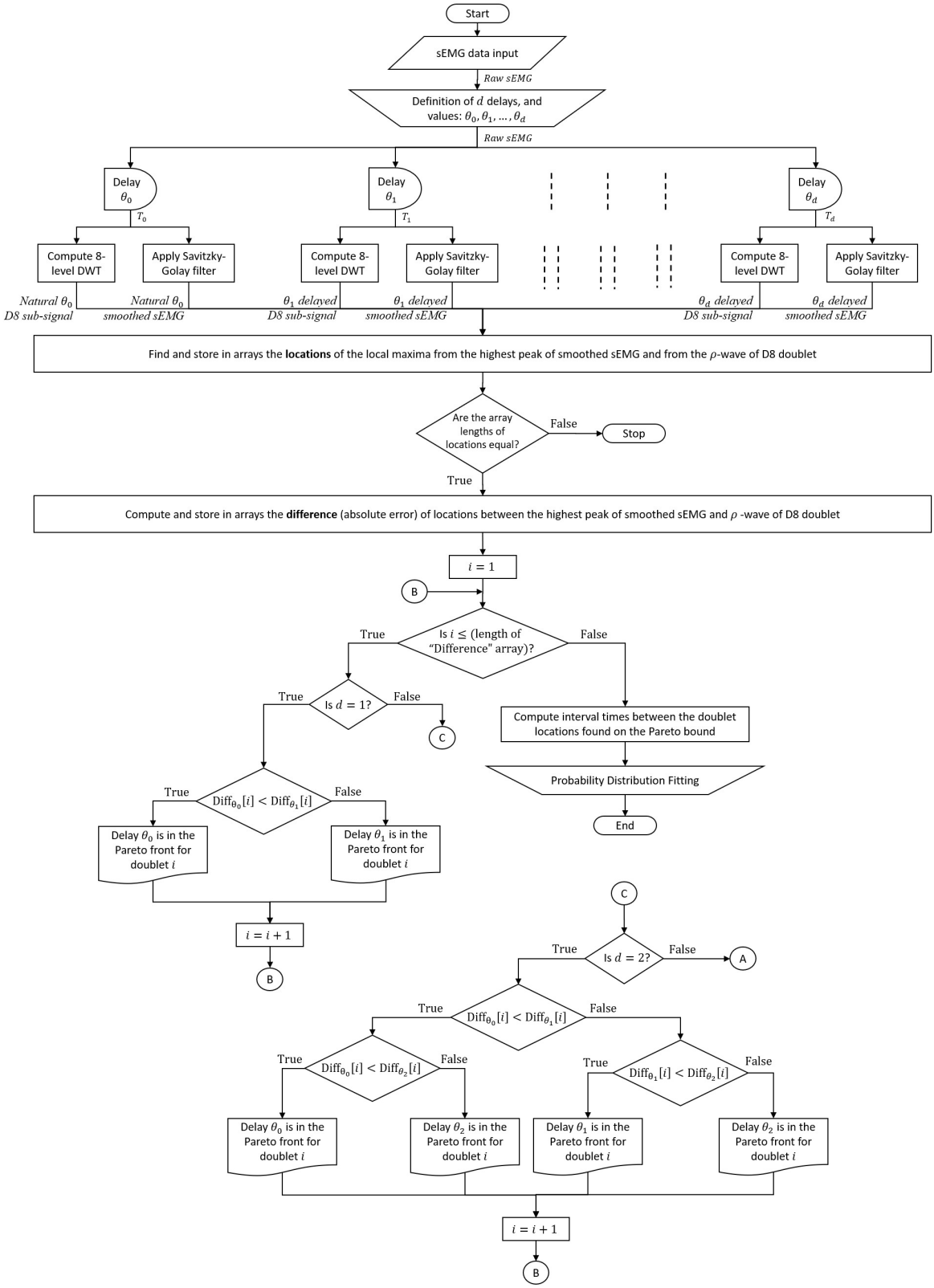
Start
sEMG data input
Raw sEMG
Definition of d delays, and values: $\theta_0, \theta_1, \ldots, \theta_d$
Raw sEMG
Delay θ_0
T_0
Delay θ_1
T_1
Delay θ_d
T_d
Compute 8-level DWT
Apply Savitzky-Golay filter
Compute 8-level DWT
Apply Savitzky-Golay filter
Compute 8-level DWT
Apply Savitzky-Golay filter
Natural θ_0 D8 sub-signal
Natural θ_0 smoothed sEMG
θ_1 delayed D8 sub-signal
θ_1 delayed smoothed sEMG
θ_d delayed D8 sub-signal
θ_d delayed smoothed sEMG
Find and store in arrays the **locations** of the local maxima from the highest peak of smoothed sEMG and from the ρ-wave of D8 doublet
Are the array lengths of locations equal?
False
Stop
True
Compute and store in arrays the **difference** (absolute error) of locations between the highest peak of smoothed sEMG and ρ -wave of D8 doublet
$i = 1$
B
Is $i \leq$ (length of "Difference" array)?
True
False
Is $d = 1$?
True
False
C
Compute interval times between the doublet locations found on the Pareto bound
Probability Distribution Fitting
End
$\text{Diff}_{\theta_0}[i] < \text{Diff}_{\theta_1}[i]$
True
False
Delay θ_0 is in the Pareto front for doublet i
Delay θ_1 is in the Pareto front for doublet i
$i = i + 1$
B
C
Is $d = 2$?
True
False
A
$\text{Diff}_{\theta_0}[i] < \text{Diff}_{\theta_1}[i]$
True
False
$\text{Diff}_{\theta_0}[i] < \text{Diff}_{\theta_2}[i]$
True
False
$\text{Diff}_{\theta_1}[i] < \text{Diff}_{\theta_2}[i]$
True
False
Delay θ_0 is in the Pareto front for doublet i
Delay θ_2 is in the Pareto front for doublet i
Delay θ_1 is in the Pareto front for doublet i
Delay θ_2 is in the Pareto front for doublet i
$i = i + 1$
B

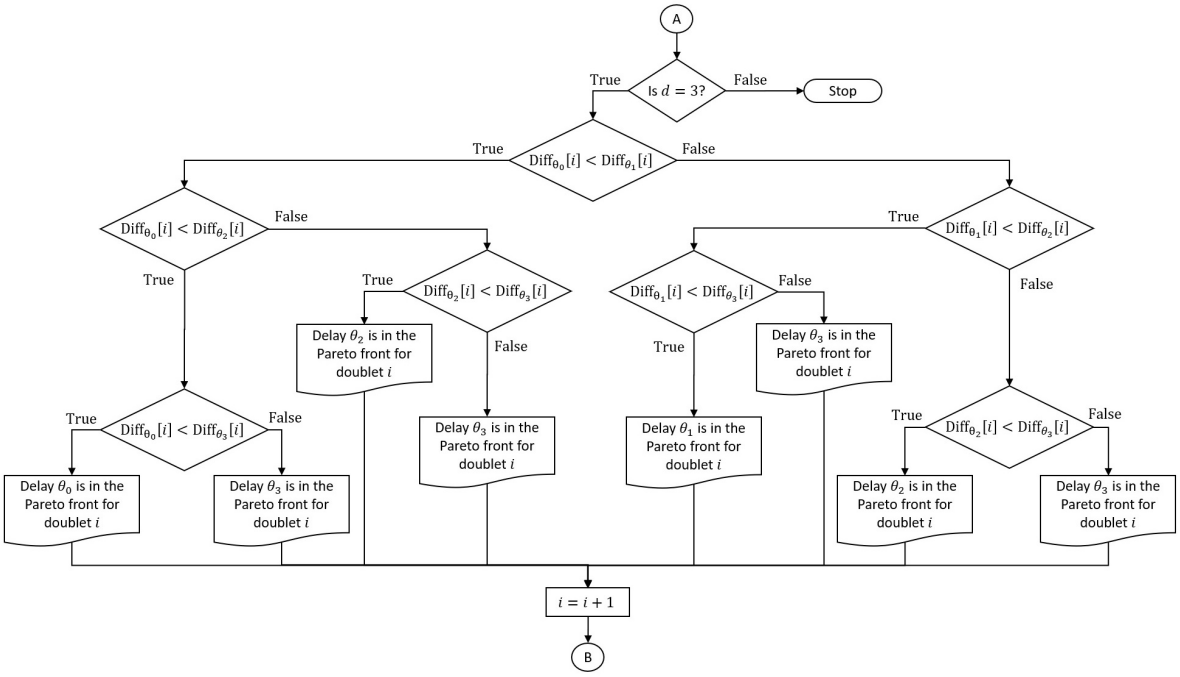

FIGURE 5

Complete sEMG signal processing and analysis flowchart: The raw sEMG signal passes through d predefined delays to time shift its 8-level sub-signal and its smoothed sEMG signal. In the example of this paper, the number of delays is $d = 3$, with values of $\theta_0 = 0$ ms, $\theta_1 = 5$ ms, $\theta_2 = 10$ ms, $\theta_3 = 15$ ms. Thus, the expert system finds the minimal errors among ρ-waves (shown in Fig. 4) between the $d + 1$ pairs of signals that come from the same sEMG trace, enhancing waveform matching and providing the Pareto front $\rho\rho$-interval times (and/or ρ-wave magnitudes) for probability distribution analysis.

3 Model selection criterion and sample size guidelines

3.1 Best fitting probability distribution

Akaike's approach to finding the best probability distribution fit is a Maximum Likelihood Estimation technique [23] that seeks to provide a measure of fitting relative to distinct probability models by estimating parameters that maximize their Likelihood function.

The corrected Akaike Information Criterion, (correction for overfitting) is defined as $AICc = AIC + \frac{2k(k+1)}{n-k-1}$, where n is the sample size, k is the number of parameters, and $AIC = 2k - 2LogLikelihood(\theta)$, where θ represents the parameters to be estimated for a given model.

Let $X_1,\ X_2,\ \ldots,\ X_n$ be a set of continuous random variables with joint density function $f_\theta(X)$ depending on the parameters θ. The $Likelihood$ function $L(\theta) = f_\theta(x_1,\ x_2,\ \ldots,\ x_n)$, sometimes written as $L(\theta|x)$, is the joint probability distribution $f_\theta(x_1,\ x_2,\ \ldots,\ x_n)$ with parameters θ of the set of n random variables evaluated at the observed values from the sample. The $LogLikelihood$ represents the natural log of the $Likelihood$ function, which is often preferred as it simplifies the calculations of critical values.

Since there is no prior knowledge of the underlying distribution of doublet return times, the AICc—by means of estimating the parameters that provide the largest plausibility for obtaining the observed values for several probability models—provides a point of comparison among the probability models that the samples are most likely to come from, serving as a means for model selection. Some of the models tested face-to-face in this sense include the Gamma, Weibull, Exponential, LogNormal, GLog, Johnson Su, Johnson Sl, Gaussian, and Normal 2 & 3 Mixture probability densities.

Akaike [23] reformulates the maximization of the $LogLikelihood$ function by working with its negative value (minimization of the $LogLikelihood$ function), in such case, lower values of AICc denote better model fits.

Since the AICc only provides a ranking among different types of distributions and does not warn for poorly fitted models, a Goodness-of-fit test for the model with the lowest AICc complements this part of the model selection technique, ensuring that the best-ranked model represents a good fit.

3.2 Sample size guidelines

To construct guidelines on the minimum and the maximum number of return times to consider in the distribution fit analysis, we performed simulations (with 5,000 trials at different sample sizes in the range from 5 to 5,000) by random sampling from an underlying distribution and obtained the number of times a given distribution was the best fit in the AICc sense.

The two-parameter Weibull distribution (α, β)

$$f(x;\alpha,\beta) = \frac{\beta}{\alpha}\left(\frac{x}{\alpha}\right)^{\beta-1} e^{-\left(\frac{x}{\alpha}\right)^{\beta}}; \qquad for\ \alpha,\beta > 0;\ x \geq 0,$$

where α and β are the scale and shape parameters, respectively, was found to be the most robust at small sample sizes as it required the smallest sample size (n) to be identified as the best fit most of the trials. For instance, Fig. 9 in the Appendix section shows that at least $n \approx 6$ samples were required to achieve ∼30-60% success rate for several parameter values of α and β, compared with Gamma $(\lambda = 4,\ scale = 1)$ with at least $n \approx 26$ with ∼32% success rate, Gaussian $\left(\mu = 100,\ \sigma^2 = 30^2\right)$ with at least $n \approx 130$ with ∼40% success rate, Normal 3 Mixture with at least $n \approx 120$ with ∼25% success rate, and Normal 2 Mixture with at least $n \approx 38$ with ∼37% success rate as shown in Fig. 10 in the Appendix section. Due to the high robustness of the Weibull distribution at small sample sizes that we observed with simulations, it is not surprising that the Weibull distribution is widely applied in reliability tests [24, 25, 26], which are often hampered with small sample sizes.

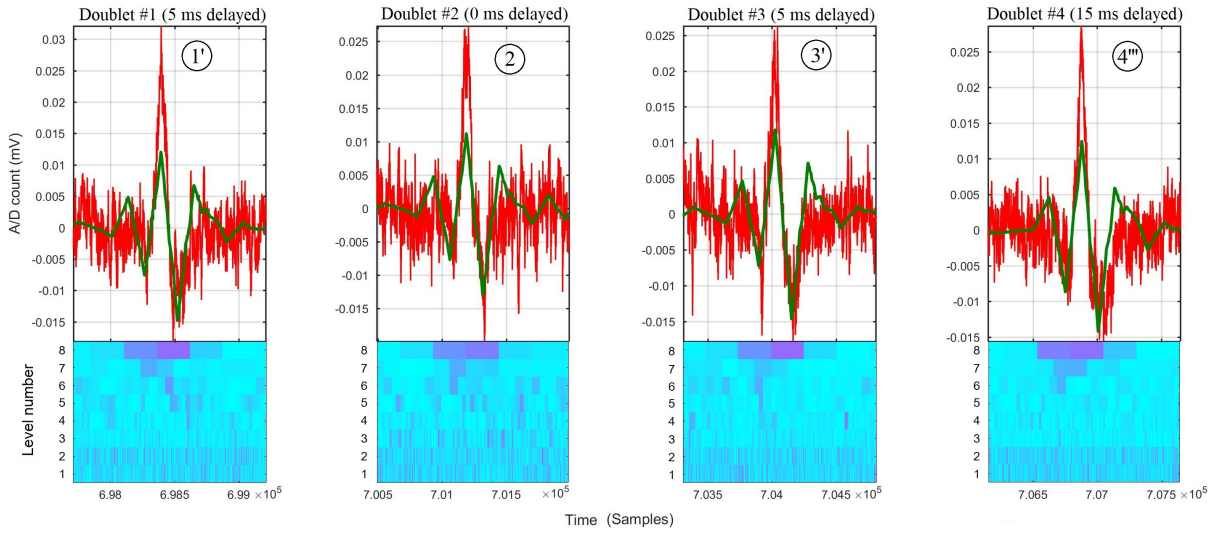

FIGURE 6

Zoom around the four bursts of raw thoracic sEMG trace (in red) of subject #4 first shown in Fig. 2, superimposed with a delayed 8-level sub-signal (in green); their respective scalogram is shown below: The D8 doublets #1', #2, #3', and #4''' correspond to time-shifting the DWT at the Pareto front time delays of 5 ms, 0 ms, 5 ms, and 15 ms, respectively, obtained for each doublet by the expert system.

As regard to the maximum number of return times to consider in the distribution fitting analysis, a stopping rule can be determined when the AICc approaches a minimum value, meaning that the percentage change of AICc approaches zero as the sample size increases as shown in Figs. 11 and 12 in the Appendix section for two different individuals.

4 Results

4.1 Results: waveform matching

Although the time locations in the first three doublets of Fig. 2 were lost in the process to retrieve the ρ-wave of D8 doublet #4, as shown in Fig. 4, the expert system recovered and found the Pareto time localization of the other doublets at each predefined delay.

With the predefined delay values inputted in the expert system for waveform matching (0, 5, 10, and 15 ms), the delays $\theta_1 = 5$ ms for doublet #1', $\theta_0 = 0$ ms for doublet #2, $\theta_1 = 5$ ms for doublet #3', and $\theta_3 = 15$ ms for doublet #4''' have been found by the expert system to be on the Pareto front (see Fig. 6).

Furthermore, the scalograms of Fig. 6, that are obtained for each burst by their respective delay times found by the expert system, also show that the $\pi\kappa\rho\sigma\tau$ wave is constructed by mainly two relatively high and successive D8 coefficients (each spanning 60 ms), correlating with our

description of a high incidence of multiple neurons firing double "exceptional" spikes [14] within each burst.

4.2 Results: theoretical probability distributions

Among the 24 paraspinal signals, the Weibull distribution was found to be the best probability fit in the AICc sense among the subjects with quadriplegia as shown in Figs. 8a and 8b; whereas the Normal 2 & 3 Mixtures were prevalently the best fit among control subjects as shown in Figs. 7a, 7b, 7c, and 7d. These results are summarized in Table 1 in the Appendix section along with the parameter estimates for the best-fitted distributions.

4.3 Results: control versus quadriplegic subjects

The contrasting difference in the results of the present study between quadriplegic and control patients, namely in their probability distributions of doublet return times and sample sizes, points to "doublets" becoming more prevalent (and with multimodal return times) in healthy neuromuscular systems than unhealthy ones. Furthermore, the more predominant rhythmic synchronization of neurophsyological activity of healthy subjects is consistent with the hypothesis that coherence at a distance is an indication of the nervous system able to coordinate the activity of many muscles [1, 9, 10].

5 Discussion

5.1 Neurophysiological personality

We hypothesize that the rhythmic bursts represent a synchronization of multiple MUs firing exceptional doublets, and that there is a probable connection between them and the dynamical system theory of the return time of rare events [27, 28] and the Generalized Extreme Value (GEV) theory of such rare events [20, 29] and the neurophysiological studies by Piotrkiewicz [14]. In the last-mentioned studies, double-firing motor units classified as single, repetitive, and exceptional doublets, constituted a small percentage (9.5%) of recorded neuronal discharges and were considered as "unusual" discharges, whereas the exceptional type was even more unusual ($\sim$1%).

In this CPG entrainment technique, those doublets deemed *exceptional* can be reproduced at will, in contrast to the studies by Piotrkiewicz [14], where the volunteers were not trained to evoke doublets.

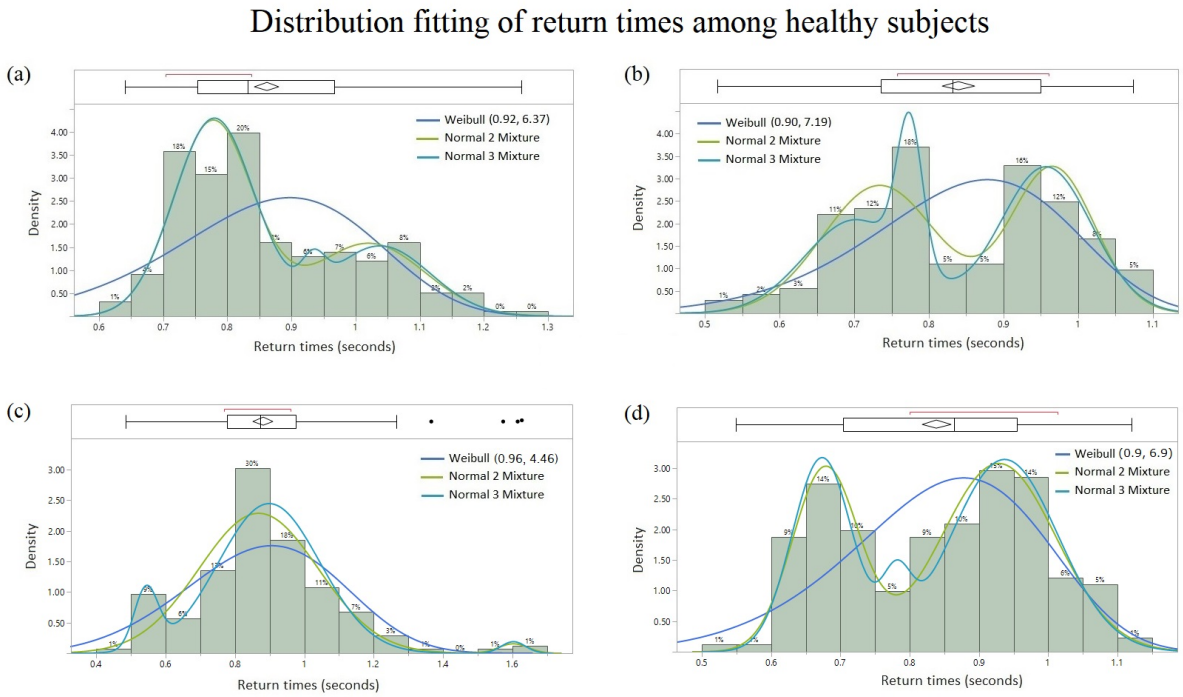

FIGURE 7

Probability distribution fitting of return times from healthy subjects: (a) lumbar spine signal of Subject #6 with Normal 2 Mixture ($AICc = -272.53$), Normal 3 Mixture ($AICc = -265.98$), and Weibull ($AICc = -199.41$), (b) sacral signal of Subject #8 with Normal 3 Mixture ($AICc = -187.61$), Normal 2 Mixture ($AICc = -186.31$), and Weibull ($AICc = -167.78$), (c) cervical signal of Subject #5 with Normal 3 Mixture ($AICc = -95.26$), Normal 2 Mixture ($AICc = -87.19$), and Weibull ($AICc = -51.56$), and (d) cervical signal of Subject #8 with Normal 2 Mixture ($AICc = -236.16$), Normal 3 Mixture ($AICc = -230.59$), and Weibull ($AICc = -194.86$). Lower AICc values indicate a better distribution fit.

5.2 Heart Rate Variability and Bursting Rate Variability

Similar to the normal resting heart rate range from 60 to 100 beats per minute [30], here the observed doublet return time rate is between 60 and 88 cycles per minute, which indicates a possible connection between HRV and BRV.

It might be argued that the repetitive sEMG bursts represent a cardiac noise artifact. However, if we were observing an electrocardiographic (ECG) artifact in the sEMG traces, then we would expect the ECG artifact to have similar time parameters as those observed in a clinical ECG. Table 3.1 in [31] shows that the typical P-wave, QRS-complex, and corrected QT-interval durations for a healthy male adult have normal values and limits of 110 ± 20 ms, 100 ± 20 ms, and 400 ± 40 ms respectively. Thus, a typical cardiac PQRST-wave duration would span a total of 510 ± 60 ms. Furthermore, Fig. 3 of [30] shows a textbook example of an ECG cycle in normal conditions with a total duration of $\sim$570 ms.

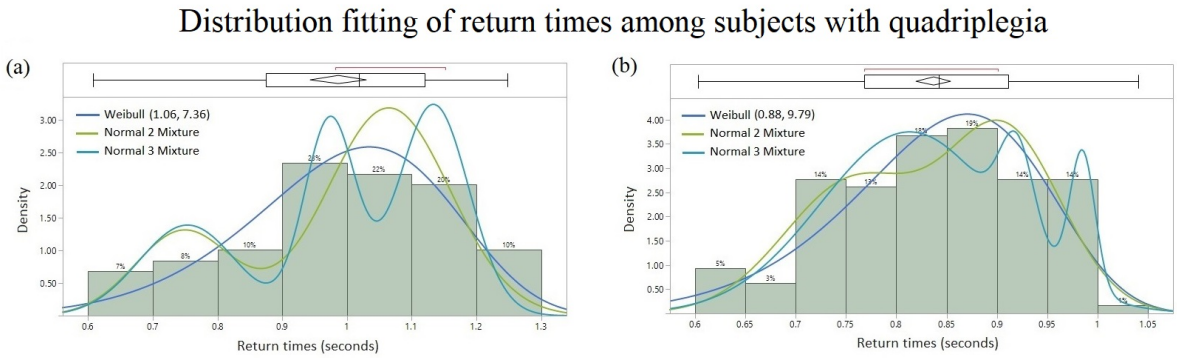

FIGURE 8

Probability distribution fitting of return times from patients with quadriplegia: (a) Thoracic signal of Subject #2 with Weibull ($AICc = -45.69$), Normal 2 Mixture ($AICc = -41.36$), and Normal 3 Mixture ($AICc = -35.46$), (b) lumbar spine signal of Subject #1 with Weibull ($AICc = -231.43$), Normal 2 Mixture ($AICc = -227.36$), and Normal 3 Mixture ($AICc = -227.12$). Lower AICc values indicate a better distribution fit.

In this sEMG phenomenon, the $\pi\kappa\rho\sigma\tau$-wave and the $\kappa\rho\sigma$-complex span shorter durations of $\sim$125 ms and $\sim$62.5 ms resp., compared with the equivalent cardiac PQRST-wave and QRS-complex durations of 510 ± 60 ms and 110 ± 20 ms resp.

Besides the difference in total wavelength between the cardiac cycle and "doublets," it is worth stressing that here variability does not appear to occur *within* the doublet (peak-dip intra-doublet time), but rather on the outside (inter-doublet return time), as the $\pi\kappa\rho\sigma\tau$ wave duration of $\sim$125 ms appears to be prevailingly fixed among doublets. This is unlike HRV, where a considerable amount of variability occurs among waves within same cardiac cycles (e.g. QT prolongation [32]).

To further exemplify the difference between a pure ECG trace and the $\pi\kappa\rho\sigma\tau$ wave found here in the sEMG traces, studies show that the return time distributions of R-waves in ECG recordings have been found Erlang in normal subjects, and a weighted average of Erlang with a second distribution (e.g. Weibull) in patients with arrhythmia [33, 34].

5.3 Off-line and On-line BRV for Biofeedback Applications

For biofeedback applications, our objective is to help quadriplegic patients recover some motor control by learning how to evoke more doublet oscillations with return time distribution deviating from Weibull towards normal mixtures.

Another objective is to conduct *on-line* assessments by means of implementing the complete *off-line* technique described in section 2.5 with real-time DWT [35]. For real-time muscle per-

formance evaluations, it would reinforce the training process to help increase the number of synchronized motor units, resulting in stronger muscle contractions [36].

The proposed technique is not restricted to only paraspinal muscles as it may span the evaluation of the neuromuscular system to a greater extent—for instance, to assess rhythmic involuntary contractions such as tremors, or uterine contractions in pregnancy. In the former, it could provide feedback to therapies in the field. In the latter, it would monitor the return times of uterine EMG bursts to potentially warn for signs of imminent, false, or preterm labor [37].

6 Conclusions

The major contribution in this paper is the identification of a new neurophysiological phenomenon—the *Bursting Rate Variability* that bears some resemblance to *Heart Rate Variability*, but that still differs from it in several respects. BRV is based on recursively shifting the Daubechies 3 wavelet transform of the raw electromyographic signal to successively exhibit perfect MUAP doublets at the D8 level.

The presence of such *doublets* in the sEMG signal has been conjectured to reveal coordination of muscle masses at a distance to achieve a higher hierarchy level movement. The return time statistic of the doublets developed here adds some quantitative insights to this observation, with *Weibull* to *normal mixture* distribution a possible indication of a quadriplegic subject recovering some motor control.

Furthermore, from this rhythmic and highly synchronized firing pattern, the neuronal connection *structure learning* is contemplated. Whereas cardiology applications, while plausible, remain to be assessed by including electrocardiogram monitoring to our protocol while recording sEMG activity simultaneously.

Finally, from a theoretical viewpoint, this research is related to the statistic of return time of a dynamical system to some subset of its state space. The more recent Generalized Extreme Value (GEV) theory, which proceeds from the statistic of the extreme value of an observable (e.g., a sEMG signal) rather than the return time of such events, could offer an alternative way to look at the same phenomenon.

7 Appendix

Acknowledgment

Dr. Fariba Ariaei's discussions on the return time distributions in HRV dynamics are gratefully acknowledged.

TABLE 1

Distribution Fit Analysis: Enhanced-Matched Doublets

Type of Subject	Subject #	Signal	Sample Size[a]	Mean[b]			Standard Deviation[b]			Best Fit[c]	Fitted Parameter Estimates			Goodness of Fit Test[d]
				Experimental	*Theoretical*	$\%_{error}$	*Experimental*	*Theoretical*	$\%_{error}$		*Type*	*Parameter*	*Estimate*	*p-value*
Quad	1	Lumbar	131	0.83679	0.83671	0.00956	0.09978	0.10269	2.83377	Weibull	Scale	α	0.8802891	0.25
											Shape	β	9.7908324	
	2	Thoracic	60	0.98695	0.98959	0.26678	0.16850	0.15875	6.14173	Weibull	Scale	α	1.0551864	0.1975
											Shape	β	7.3575348	
Control	3	Cervical	297	0.79074	0.79074	0.00073	0.07175	0.06955	3.16109	Normal 2 Mixture	Location	μ_1	0.7582432	0.4727
											Location	μ_2	0.7990039	
											Dispersion	σ_1	0.1110593	
											Dispersion	σ_2	0.0509513	
											Probability	π_1	0.2026008	
											Probability	π_2	0.7973992	
		Thoracic	142	0.80970	0.80969	0.00119	0.05908	0.05819	1.52254	Normal 3 Mixture	Location	μ_1	0.7433704	0.4605
											Location	μ_2	0.8374764	
											Location	μ_3	1.0203324	
											Dispersion	σ_1	0.0261000	
											Dispersion	σ_2	0.0302071	
											Dispersion	σ_3	0.0200882	
											Probability	π_1	0.3226223	
											Probability	π_2	0.6632976	
											Probability	π_3	0.0140801	
		Lumbar	183	0.68051	0.68050	0.00090	0.08635	0.08508	1.49601	Normal 3 Mixture	Location	μ_1	0.4872577	0.4652
											Location	μ_2	0.6821022	
											Location	μ_3	0.9507306	
											Dispersion	σ_1	0.0116068	
											Dispersion	σ_2	0.0720919	
											Dispersion	σ_3	0.0171289	
											Probability	π_1	0.0299150	
											Probability	π_2	0.9543367	
											Probability	π_3	0.0157483	
		Sacral	257	0.71217	0.71215	0.00245	0.09731	0.09614	1.21324	Normal 2 Mixture	Location	μ_1	0.7089589	0.4707
											Location	μ_2	1.1198451	
											Dispersion	σ_1	0.0894392	
											Dispersion	σ_2	0.0236820	
											Probability	π_1	0.9922274	
											Probability	π_2	0.0077726	
	4	Cervical	1,055	0.69755	0.69756	0.00088	0.04814	0.04753	1.28368	Normal 3 Mixture	Location	μ_1	0.5211892	0.4855
											Location	μ_2	0.7008101	
											Location	μ_3	0.6990413	
											Dispersion	σ_1	0.0106487	
											Dispersion	σ_2	0.0186435	
											Dispersion	σ_3	0.0974058	
											Probability	π_1	0.0166192	
											Probability	π_2	0.8313767	
											Probability	π_3	0.1520042	
		Thoracic	1,550	0.69693	0.69693	0.00001	0.02918	0.02857	2.12082	Normal 3 Mixture	Location	μ_1	0.6663625	0.4881
											Location	μ_2	0.6998140	
											Location	μ_3	0.6913961	
											Dispersion	σ_1	0.0868998	
											Dispersion	σ_2	0.0165026	
											Dispersion	σ_3	0.0331125	
											Probability	π_1	0.0507722	
											Probability	π_2	0.8083748	
											Probability	π_3	0.1408530	

Statistical comparison of inter-burst interval times between quadriplegic and control subjects with the enhanced-matched procedure.

[a] Sample size is the number of doublet return times obtained with the expert system.

[b] Units of mean and standard deviation are in seconds.

[c] Model selection criterion was based on the lowest AICc value.

[d] Goodness-of-fit tests for Weibull and Normal Mixtures were Cramer-von Mises W and Pearson's chi-squared tests respectively.

Type of Subject	Subj. #	Signal	Sample Size[a]	Mean[b]			Standard Deviation[b]			Best Fit[c]	Fitted Parameter Estimates			Goodness of Fit Test[d]
				Experimental	*Theoretical*	$\%_{error}$	*Experimental*	*Theoretical*	$\%_{error}$		*Type*	*Parameter*	*Estimate*	*p-value*
Control	4	Lumbar	544	0.69361	0.69361	0.00050	0.03051	0.03020	1.01183	Normal 3 Mixture	Location	μ_1	0.5177513	0.4798
											Location	μ_2	0.6904178	
											Location	μ_3	0.7028590	
											Dispersion	σ_1	0.0077241	
											Dispersion	σ_2	0.0128245	
											Dispersion	σ_3	0.0356578	
											Probability	π_1	0.0091908	
											Probability	π_2	0.6063979	
											Probability	π_3	0.3844114	
		Sacral	265	0.71434	0.71434	0.00057	0.06640	0.06549	1.39002	Normal 3 Mixture	Location	μ_1	0.5062527	0.4711
											Location	μ_2	0.6927545	
											Location	μ_3	0.7269021	
											Dispersion	σ_1	0.0228841	
											Dispersion	σ_2	0.0117517	
											Dispersion	σ_3	0.0636254	
											Probability	π_1	0.0223802	
											Probability	π_2	0.2231447	
											Probability	π_3	0.7544751	
	5	Cervical	179	0.88047	0.88045	0.00200	0.19756	0.19505	1.28573	Normal 3 Mixture	Location	μ_1	0.5437492	0.4648
											Location	μ_2	0.8985177	
											Location	μ_3	1.6026796	
											Dispersion	σ_1	0.0343333	
											Dispersion	σ_2	0.1466987	
											Dispersion	σ_3	0.0351786	
											Probability	π_1	0.0841804	
											Probability	π_2	0.8990634	
											Probability	π_3	0.0167563	
		Lumbar	199	0.96771	0.96771	0.00049	0.20595	0.19590	5.12965	Normal 2 Mixture	Location	μ_1	0.9899384	0.4667
											Location	μ_2	0.9611284	
											Dispersion	σ_1	0.3388004	
											Dispersion	σ_2	0.1248396	
											Probability	π_1	0.2282849	
											Probability	π_2	0.7717151	
		Sacral	361	1.00026	1.00025	0.00064	0.24514	0.24297	0.89479	Normal 2 Mixture	Location	μ_1	0.9255663	0.4753
											Location	μ_2	1.4218577	
											Dispersion	σ_1	0.1636967	
											Dispersion	σ_2	0.1782215	
											Probability	π_1	0.8495092	
											Probability	π_2	0.1504908	
	6	Thoracic	285	0.87775	0.87776	0.00069	0.17501	0.17362	0.79960	Normal 2 Mixture	Location	μ_1	0.6472983	0.4721
											Location	μ_2	0.9608497	
											Dispersion	σ_1	0.0912896	
											Dispersion	σ_2	0.1093363	
											Probability	π_1	0.2650080	
											Probability	π_2	0.7349920	
		Lumbar	202	0.86156	0.86156	0.00008	0.13750	0.13609	1.03961	Normal 2 Mixture	Location	μ_1	0.7772509	0.4669
											Location	μ_2	1.0203541	
											Dispersion	σ_1	0.0616972	
											Dispersion	σ_2	0.0873302	
											Probability	π_1	0.6531933	
											Probability	π_2	0.3468067	
		Sacral	144	0.87099	0.87099	0.00034	0.13305	0.13092	1.62844	Normal 2 Mixture	Location	μ_1	0.7801195	0.4608
											Location	μ_2	0.9987842	
											Dispersion	σ_1	0.0563301	
											Dispersion	σ_2	0.0940075	
											Probability	π_1	0.5844435	
											Probability	π_2	0.4155565	

References

[1] E. Jonckheere, P. Lohsoonthorn, S. Musuvathy, V. Mahajan, and M. Stefanovic. On a standing wave Central Pattern Generator and the coherence problem. *Biomedical Signal Processing and Control*, pages 336–347, 2010.

[2] R. Martin del Campo and Edmond Jonckheere. Stationary regime for Standing Wave Central Pattern Generator. In *3rd IEEE Global Conference on Signal and Information Pro-*

Type of Subject	Subj. #	Signal	Sample Size[a]	Mean[b]			Standard Deviation[b]			Best Fit[c]	Fitted Parameter Estimates			Goodness of Fit Test[d]
				Experimental	*Theoretical*	$\%_{error}$	*Experimental*	*Theoretical*	$\%_{error}$		*Type*	*Parameter*	*Estimate*	*p-value*
Control	7	Lumbar	224	0.79185	0.79185	0.00037	0.16560	0.16096	2.88156	Normal 2 Mixture	Location	μ_1	0.7358333	0.4686
											Location	μ_2	0.9235629	
											Dispersion	σ_1	0.0766122	
											Dispersion	σ_2	0.2197815	
											Probability	π_1	0.7016254	
											Probability	π_2	0.2983746	
		Sacral	125	0.73425	0.73424	0.00156	0.09611	0.09418	2.05266	Normal 2 Mixture	Location	μ_1	0.7148177	0.4579
											Location	μ_2	0.8971440	
											Dispersion	σ_1	0.0795113	
											Dispersion	σ_2	0.0231078	
											Probability	π_1	0.8934829	
											Probability	π_2	0.1065171	
	8	Cervical	183	0.83867	0.83868	0.00104	0.14154	0.14027	0.90740	Normal 2 Mixture	Location	μ_1	0.6780456	0.4652
											Location	μ_2	0.9284455	
											Dispersion	σ_1	0.0476830	
											Dispersion	σ_2	0.0831964	
											Probability	π_1	0.3584937	
											Probability	π_2	0.6415063	
		Thoracic	222	0.85704	0.85704	0.00032	0.13054	0.12937	0.90700	Normal 2 Mixture	Location	μ_1	0.7333043	0.4684
											Location	μ_2	0.9528567	
											Dispersion	σ_1	0.0714954	
											Dispersion	σ_2	0.0685575	
											Probability	π_1	0.4364308	
											Probability	π_2	0.5635692	
		Lumbar	339	0.77260	0.77259	0.00071	0.12678	0.12602	0.60054	Normal 2 Mixture	Location	μ_1	0.7135704	0.4745
											Location	μ_2	0.9533303	
											Dispersion	σ_1	0.0753422	
											Dispersion	σ_2	0.0616300	
											Probability	π_1	0.7538200	
											Probability	π_2	0.2461800	
		Sacral	146	0.83955	0.83956	0.00106	0.13539	0.13373	1.24495	Normal 3 Mixture	Location	μ_1	0.7022492	0.4611
											Location	μ_2	0.7743037	
											Location	μ_3	0.9565682	
											Dispersion	σ_1	0.0689697	
											Dispersion	σ_2	0.0171418	
											Dispersion	σ_3	0.0612079	
											Probability	π_1	0.3609125	
											Probability	π_2	0.1383833	
											Probability	π_3	0.5007042	
	9	Thoracic	334	0.83843	0.83843	0.00020	0.10321	0.10253	0.66653	Normal 2 Mixture	Location	μ_1	0.7648442	0.4743
											Location	μ_2	0.9331420	
											Dispersion	σ_1	0.0649377	
											Dispersion	σ_2	0.0517103	
											Probability	π_1	0.5627745	
											Probability	π_2	0.4372255	
		Lumbar	307	0.83850	0.83849	0.00773	0.10641	0.10565	0.71589	Normal 2 Mixture	Location	μ_1	0.7694860	0.4732
											Location	μ_2	0.9435923	
											Dispersion	σ_1	0.0710122	
											Dispersion	σ_2	0.0467439	
											Probability	π_1	0.6036399	
											Probability	π_2	0.3963601	

cessing (Global SIP 2015), 14-16 Dec. 2015, Orlando, Florida, USA, Symposium on Signal Processing and Mathematical Modeling of Biological Processes with Applications to Cyber-Physical Systems for Precise Medicine. IEEE, February 2016. DOI: 10.1109/GlobalSIP.2015.7418330.

[3] R. Martin del Campo and Edmond Jonckheere. Stationary versus bifurcation regime for standing wave central pattern generator. *Biomedical Signal Processing and Control*, 32:57–68, 2017.

[4] E. Marder and D. Bucher. Central pattern generators and the control of rhythmic move-

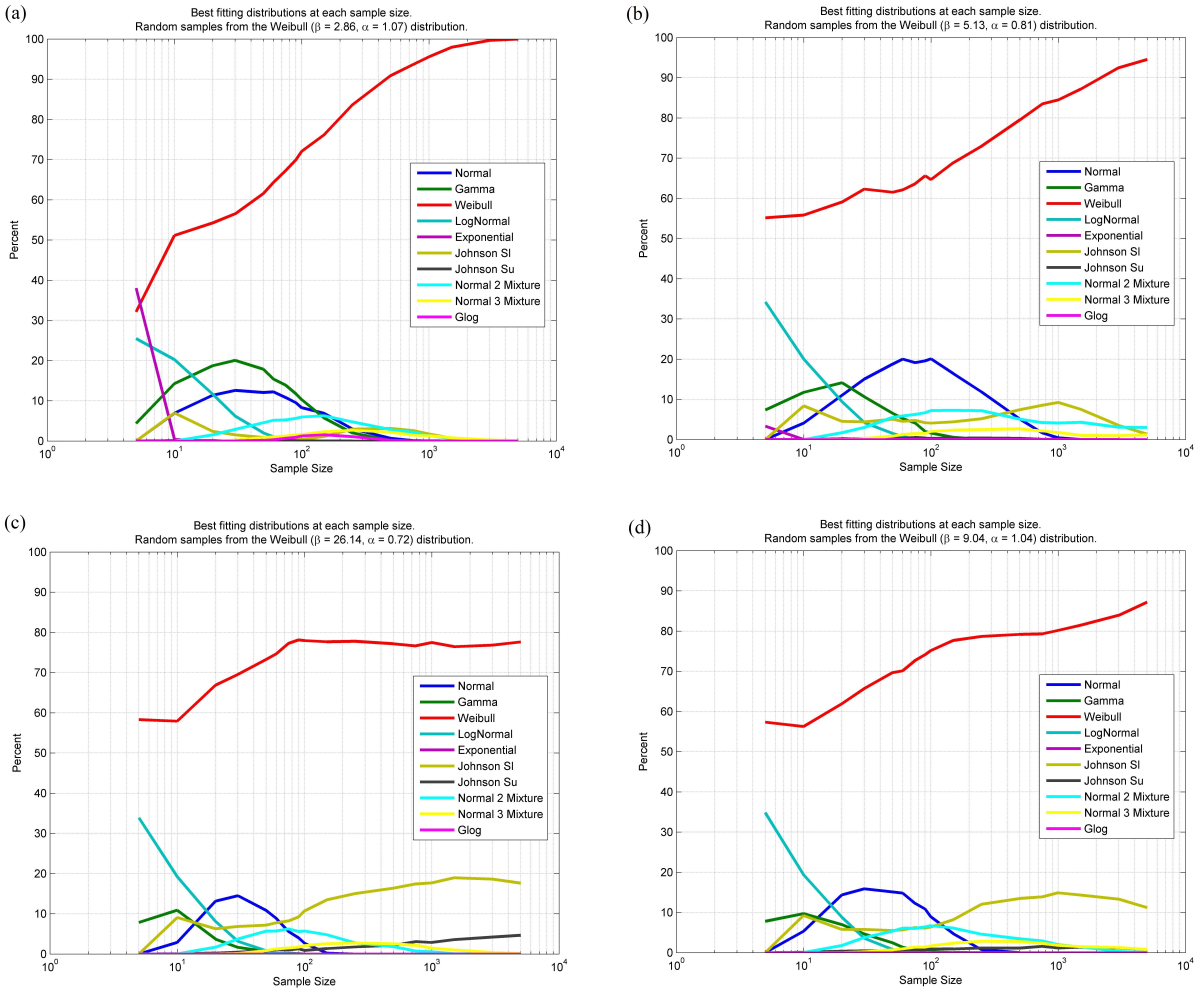

FIGURE 9

Simulation of best fitting distributions at different sample sizes obtained with the smallest AICc value by randomly sampling from (a) the Weibull ($\beta = 2.86$, $\alpha = 1.07$) distribution, (b) the Weibull ($\beta = 5.13$, $\alpha = 0.81$) distribution, (c) the Weibull ($\beta = 26.14$, $\alpha = 0.72$) distribution, and (d) the Weibull ($\beta = 9.04$, $\alpha = 1.04$) distribution.

ments. *Current Biology*, 11:986–996, 2001.

[5] E. Marder and R. L. Calabrese. Principles of Rhythmic Motor Pattern Generation. *Physiological Reviews*, 76(3), 1996.

[6] Edmond Jonckheere and Poonsuk Lohsoonthorn. Spatio-temporal analysis of an electrophysiological wave phenomenon. In *16th International Symposium on Mathematical Theory of Networks and Systems (MTNS'2014)*, Leuven, Belgium, July 5-9 2004.

[7] S. Musuvathy and E. Jonckheere. Evidence of spatio-temporal transition to chaos in the spine. In *4th International Symposium on Communications, Control, and Signal Processing*. IEEE, March 2010.

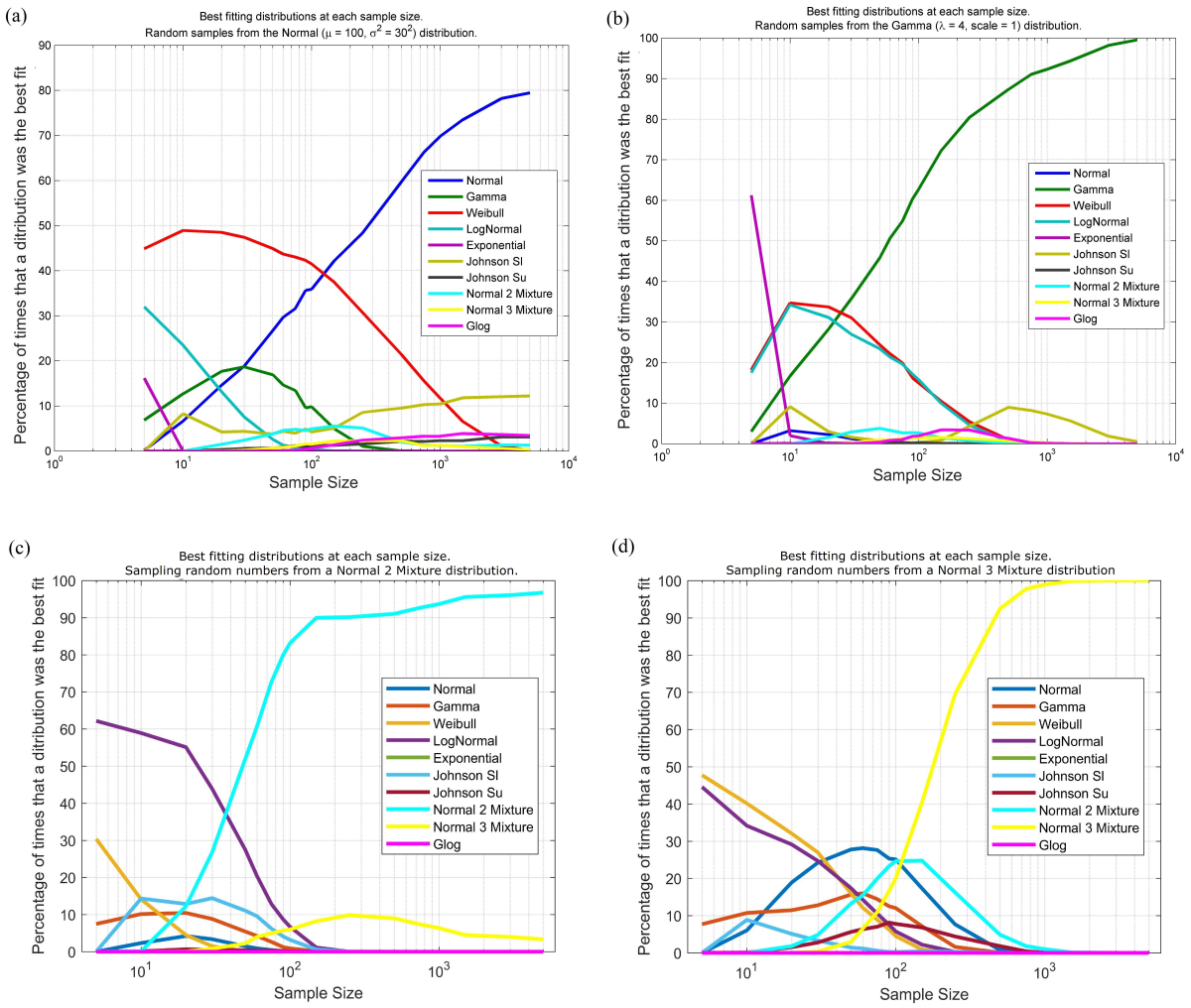

FIGURE 10

Simulation of best fitting distributions at different sample sizes obtained with the smallest AICc value by sampling random numbers from (a) the Normal ($\mu = 100$, $\sigma^2 = 30^2$) distribution, (b) the Gamma ($\lambda = 4$, $scale = 1$) distribution, (c) a Normal 2 Mixture distribution, and (d) a Normal 3 Mixture distribution.

[8] N. Kopell. We Got Rhythm: Dynamical Systems of the Nervous System. *Notice of the AMS 47*, pages 6–16, 2000.

[9] S. F. Farmer. Rhythmicity, synchronization and binding in human and primate motor systems. *The Journal of Physiology*, 509:3–14, 1998.

[10] Simon F. Farmer, John Gibbs, David M. Halliday, Linda M. Harrison, Leon M. James, Margaret J. Mayston, and John A. Stephens. Changes in EMG coherence between long and short thumb abductor muscles during human development. *The Journal of Physiology*, 579.2:389–402, 1998.

[11] B. I. Daubechies. Ten Lectures of Wavelets. Springer-Verlag, 1992. Chap. 3: Discrete

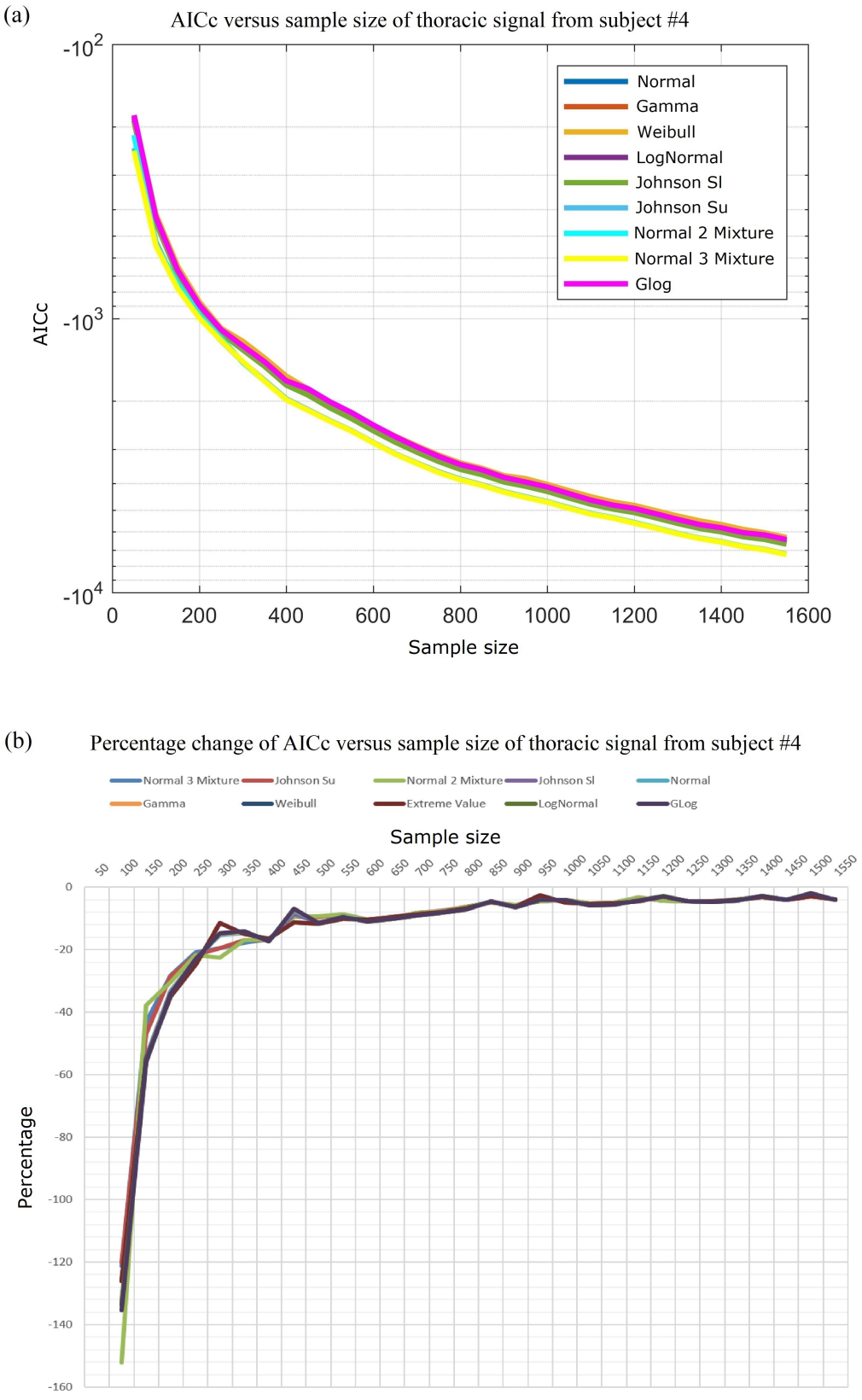

FIGURE 11

(a) AICc values versus sample size (n) to determine a stopping rule of n for thoracic signal of subject #4.

(b) Percentage change of AICc values at different sample sizes for thoracic signal of subject #4

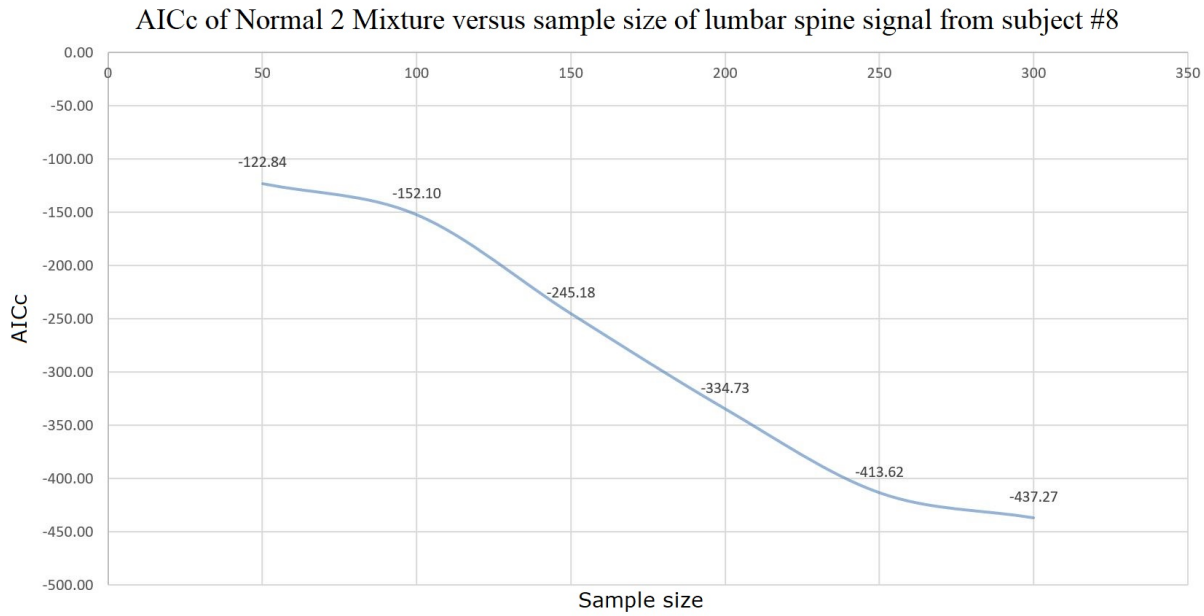

FIGURE 12

AICc values versus sample size (n) to determine a stopping rule of n for lumbar signal of subject #8.

Wavelet transforms.

[12] S. G. Mallat. A Theory for Multiresolution Signal Decomposition: The Wavelet Representation. *IEEE Transactions on Pattern Analysis and Machine Intelligence*, 11(7), 1989.

[13] J. R. Cram, G. S. Kasman, and J. Holtz. Introduction to Surface Electromyography. Aspen, 1998.

[14] M. Piotrkiewicz, O. Sebik, E. Binboga, D. Mlozniak, B. Kuraszkiewicz, and K. S. Turker. Double discharges in human soleus muscle. *Frontiers in Human Neuroscience*, 2013.

[15] W. Mlrowczynski, J. Celichowski, R. Raikova, and P. Krutki. Physiological consequences of doublet discharges on motoneuronal firing and motor unit force. *Frontiers in Cellular Neuroscience*, 2015.

[16] P. Bawa and B. Calancie. Repetitive doublets in human flexor carpi radialis muscle. *Journal of Physiology*, 339:123–132, 1983.

[17] The AANEM Nomenclature Committee. AANEM Glossary of Terms in Neuromuscular and Electrodiagnostic Medicine, 2015.

[18] I. Rodriguez-Carreño, L Gila-Useros, and A. Malanda-Trigeros. Motor Unit Action Potential Duration: Measurement and Significance. *Advances in Clinical Neurophysiology*, pages 336–347, 2012. Chap. 7.

[19] Davide Faranda, Valerio Lucarini, Giorgio Turchetti, and Sandro Vaienti. Generalized Extreme Value distribution parameters as dynamical indicators of Stability. *International Journal of Bifurcation and Chaos*, 22(11), 2012.

[20] Ana Cristina Moreira Freitas, Jorge Milhazes Freitas, and Mike Todd. Extreme Value Laws in Dynamical Systems for Non-smooth Observations. *Journal of Statistical Physics*, 142(1):108–126, 2011.

[21] W. M. Sloboda and V. M. Zatsiorsky. Wavelet analysis of EMG signals. In *Twenty-First Annual Meeting of the American Society of Biomechanics*, September 1997.

[22] A. P. Bradley. Shift-Invariance in the Discrete Wavelet Transform. In *Proc. VIIth Digital Image Computing: Techniques and Applications, 10-12 Dec 2003, Sydney*.

[23] H. Akaike. A new look at the Statistical Model Identification. *IEEE Trans. Automatic Control*, 19:716–723, 1974.

[24] Ping Jiang, Yunyan Xing, Xiang Jia, and Bo Guo. Weibull Failure Probability Estimation Based on Zero-Failure Data. *Mathematical Problems in Engineering*, 2015.

[25] K. Hisada and F. Arizino. Reliability tests for Weibull distribution with varying shape-parameter, based on complete data. *IEEE Transactions on Reliability*, 51(3):331–336, 2002.

[26] Ming-Wei Lu and Cheng Julius Wang. Weibull Data Analysis with Few or no Failures. *Recents Advances in Reliability and Quality in Design*, pages 201–210, 2008.

[27] N. Haydn, Y. Lacroix, and S. Vaienti. Hitting and return times in ergodic dynamical systems. *The Annals of Probability*, 33(5):2043–2050, 2005.

[28] Nicolai Haydn, Nicole Winterberg, and Roland Zweimüller. Return-time statistics, Hitting-time statistics and Inducing. In *Ergodic Theory, Open Dynamics, and Coherent Structures*, r 2014.

[29] Ana Cristina Moreira Freitas, Jorge Milhazes Freitas, and Mike Todd. Hitting time statistics and extreme value theory. *Probability Theory and Related Fields*, 147(3-4):675–710, 2010.

[30] A. Peterkova and M. Stremy. The raw ECG signal processing and the detection of QRS complex. In *2015 IEEE European Modelling Symposium*. IEEE, January 2015. DOI: 10.1109/EMS.2015.80.

[31] Gari D. Clifford, Francisco Azuaje, and Patrick E. McSharry. Advanced Methods and Tools for ECG Analysis. 2006. Ch. 3: ECG Statistics, Noise, Artifacts, and Missing Data.

[32] Pieter G. Postema and Arthur A.M Wilde. The Measurement of the QT Interval. *Current Cardiology Reviews*, 10:287–294, 2014.

[33] F. Ariaei, E. Jonckheere, W. Stuppy, and T. S. Callahan. Return Time of Heart Dynamics. In *European Congress for Medical and Biological Engineering (EMBEC), November 23-27, 2008, Antwerpen, Belgium*. Mathematical Biology, Contribution Session 30.

[34] F. Ariaei, E. Jonckheere, and R. Berger. Mixing Dynamics of Heart Rate Variability. In *Cardiology Research and Clinical Developments*, pages 131–142. Nova Publications, 2015. Chap. 6.

[35] A. A. Jaber and R. Bicker. Real-Time Wavelet Analysis of a Vibration Signal Based on Arduino-UNO and LabVIEW. *International Journal of Materials Science and Engineering*, 3(1), 2015.

[36] John G. Semmler. Motor Unit Synchronization and Neuromuscular Performance. *Exercise and Sport Sciences Reviews*, 30(1):8–14, 2002.

[37] Miha Lucovnik, Ruben J. Kuon, Linda R. Chambliss, William L. Maner, Shao-Qing Shi, Leili Shi, James Balducci, and Robert E. Garfield. Use of uterine electromyography to diagnose term and preterm labor. *Acta Obstetricia et Gynecologica Scandinavica*, 90(2):150–157, 2011.